CoRdE: Cosserat Rod Elements for the Dynamic Simulation of One-Dimensional Elastic Objects

J. Spillmann   M. Teschner

Computer Graphics, University of Freiburg, Germany

Abstract

Simulating one-dimensional elastic objects such as threads, ropes or hair strands is a difficult problem, especially if material torsion is considered. In this paper, we present CoRdE(french 'rope'), a novel deformation model for the dynamic interactive simulation of elastic rods with torsion. We derive continuous energies for a dynamically deforming rod based on the Cosserat theory of elastic rods. We then discretize the rod and compute energies per element by employing finite element methods. Thus, the global dynamic behavior is independent of the discretization. The dynamic evolution of the rod is obtained by numerical integration of the resulting Lagrange equations of motion. We further show how this system of equations can be decoupled and efficiently solved.
Since the centerline of the rod is explicitly represented, the deformation model allows for accurate contact and self-contact handling. Thus, we can reproduce many important looping phenomena. Further, a broad variety of different materials can be simulated at interactive rates. Experiments underline the physical plausibility of our deformation model.

Categories and Subject Descriptors (according to ACM CCS):   I.3.7 [Computer Graphics]: Three-Dimensional Graphics and Realism: Animation

Keywords: Physically-based modeling, Lagrangian dynamics, Elastic rods, Cosserat theory

1. Introduction

Physically-based modeling of elastic objects has always been an active research area in computer graphics. In the past, approaches have been proposed to model one-, two- and three-dimensional elastic objects. Elastic objects whose configuration space is one-dimensional play an important role in many research fields, e. g. in engineering or microbiology. In computer animation, one-dimensional objects represent threads, ropes or hair strands. These objects are consistently denoted as *elastic rods*, independent of their actual material properties.

Despite the fact that the configuration space of a rod has only one dimension, its mathematical representation is difficult. This comes from the observation that an elastic rod can not only bend or stretch, but also twist around its centerline. Thus, the configuration of a deformed rod can not be described in terms of the position of its centerline alone. Instead, the orientation of each cross-section introduces an additional degree of freedom. Since the positions and orientations are mechanically coupled, a rod is an intrinsically constrained system. In the late 19th century, the Cosserat brothers introduced a theory for elastic rods. Nowadays, this approach has become a fundamental part of nonlinear elasticity theory.

In computer graphics, many approaches have been presented that model elastic rods with unoriented mass-spring

chains without torsion [BLM04]. However, many important nonlinear effects such as bifurcation or out-of-plane buckling (see Fig. 1) arise solely due to the presence of torsional torques. Recently, approaches have been proposed that employ the Cosserat theory of elastic rods to handle the dynamics of hair strands or catheters in virtual surgery [BAC*06,Pai02]. These approaches result in boundary value problems that can be solved by employing shooting methods. They are, however, less suitable for handling contacts and self-contacts. Still, many effects such as looping phenomena require a robust handling of self-contacts, as illustrated in Fig. 1.

Our contribution. We propose CoRdE, a physically-based deformation model for one-dimensional elastic objects with torsion that is inspired by the Cosserat theory of elastic rods. Our deformation model can be used to simulate a broad variety of materials, ranging from flexible structures such as threads, ropes or hair strands to stiff objects with intrinsic bending and torsion such as springs or wires. We formulate the continuous kinetic, potential and dissipation energy for the elastic rod based on quaternion algebra. To simulate the rod dynamics, we discretize the rod into elements. From the continuous energies, we derive discrete energies by employing finite element methods. As a consequence, the global behavior of the rod is independent of the discretization. The equations of motion are obtained by taking variations of the Lagrangian. We then show how to
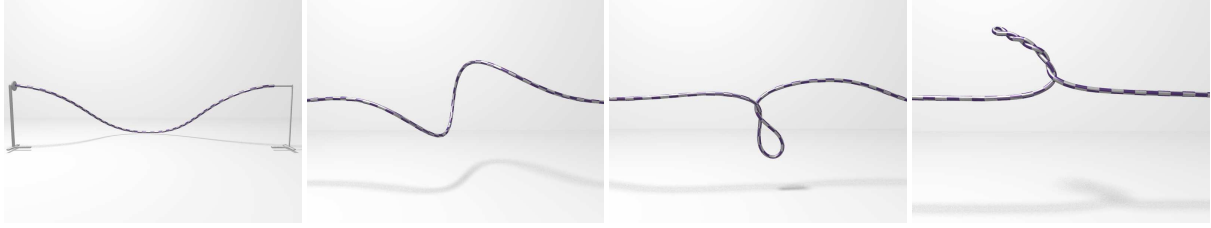
Figure 1: *Dynamic looping phenomenon of a rod under torsional strain: A rod is spanned between two anchors, and its ends are clamped. A torque transducer on the left varies the end-to-end rotation of the rod. We observe a bifurcation sequence that results in a looping with an increasing number of self-contacts. This behavior can not be reproduced by approaches that do not consider material torsion.*

decouple the resulting system of equations in order to solve it directly. In addition, we model the internal friction such that the rigid body motion of the rod is not affected.

In contrast to existing approaches that simulate the rod by solving a boundary value problem, e. g. [BAC*06, Pai02], we can handle complex collision and self-collision configurations. Thus, our deformation model enables the dynamic simulation of knots and looping phenomena. Moreover, the approach is elegant and simple to implement, and since it is linear in the number of nodes, ropes and threads can be animated at interactive rates.

Organization. After discussing the previous work, we give in Section 3 a short introduction of the Cosserat model for elastic rods that is essential for an understanding of our approach. Further, we derive expressions for the continuous potential, kinetic and dissipation energy of the deforming rod. In order to numerically simulate the rod, it is necessary to discretize it into elements, as discussed in Section 4. The potential, kinetic and dissipation energy of each element is then expressed in terms of the continuous energies. This section results in the discrete equations of motion for the rod. These equations could be solved by employing iterative numerical methods. However, this can not be done at interactive rates. Thus, we discuss in Section 5 how to decouple the system of equations such that it can be solved directly. This will include some important simplifications of the problem that result in an elegant and fast method. In Section 6, we evaluate our deformation model with respect to physical plausibility and applicability.

2. Related work

The Cosserat theory of elastic rods is well-investigated in the field of nonlinear elasticity. A comprehensive discussion of the topic is given in the book of Antman [Ant95]. Amongst others, Cosserat rods are used in robotics, micro-electronic mechanical systems [CLW06], and in computational biology to model the mechanics of DNA molecules [MM96].

In physics, most approaches deal with the analysis of elastic rod equilibria, assuming that the rods are unshearable and inextensible. The definition of a position and an orientation of the start and end point of the rod results in a boundary value problem (BVP). The analysis and numerical solution of the corresponding system of ordinary differential equations is discussed in, e. g., [Keh97]. The analysis of the dynamics of inextensible rods is considered in, e. g., [Dic94]. Our approach is inspired by finite element methods based

on the Cosserat theory, notably by the works of Simo et al. [Sim85] and Cao et al. [CLW06]. In contrast to these works, we gain efficiency and simplicity by decoupling the resulting system of equations.

Physically-based simulation and animation of deformable objects is an important research area in computer graphics. A good overview on the topic is given in [NMK*05]. Physically-based animation of solids is also discussed in [MG04]. There exist two different classes of approaches to simulate and animate elastic rods, namely by considering the rod as a chain of linear objects, or by considering the rod as a curve in space. E. g. Chang et al. [CJY02] proposed an approach that is focused on hair interactions, where the hair strand is modeled from clusters linked by bending springs. Brown et al. [BLM04] published an approach to simulate knotting of ropes, including a robust collision handling scheme. They model the rope from a chain of masses and springs. However, in contrast to our deformation model, neither of these models is able to handle torsional torques. A deformable model that handles torsional torques has been presented by Wang et al. [WBD*05]. Similar to [BLM04], they model a thread from a chain of springs. In addition, they link the segments by torsional springs. In contrast to their work, we employ an energy-based approach to compute the restoration forces. Recently, Hadap [Had06] describes a methodology based on differential algebraic equations to simulate chain of rigid bodies that includes torsional stiffness dynamics. In turn, this approach is computationally expensive and thus less suitable for interactive applications.

Pioneering work in modeling elastic rods from curves has been done by Terzopoulos [TPBF87] by proposing the energy formulation of the curve in space subject to geometric deformation. Later, Qin and Terzopoulos [QT96] proposed a physically-based deformation model of a NURBS curve. They derive continuous kinetic and deformation energies, and evolve the curve by employing Lagrangian mechanics. A finite element analysis enables the simulation of the curve at interactive rates. Similar in spirit is the approach of Remion et al. [RNG00]. They employ successions of spline segments to model knitted cloth. In contrast to [QT96], they consider the control points as the degrees of freedom of the continuous object. The use of splines was also suggested by Lenoir et al. and by Phillips et al. [LMGC02, PLK02] in order to model threads. These approaches can also handle complex collision configuration. However, they have in common that material torsion can not be represented. In contrast,

our deformable model handles both bending and torsion of rods in contact.

The Cosserat theory for elastic rods has first been introduced to the community by Pai in 2002 [Pai02]. He models the statics of thin deformable structures such as catheters or sutures. He assumes the rod to be unshearable and inextensible. The configuration of the rod is obtained by solving the resulting BVP. This approach provides an efficient and physically correct way to animate continuous elastic rods. However, the model does not handle dynamics. Furthermore, self-contact and interactions require numerically sensitive shooting techniques to solve the differential equations.

Recently, Bertails et al. [BAC*06] proposed an important extension of Pai's work. Their approach is a combination of a discrete and a continuous model. They simulate hair strands as chains of helical segments. Similar to the classical Cosserat rod model, they define appropriate start and end conditions. The dynamics of the super-helices are obtained by feeding the Lagrangian equation of motion with the appropriate energy terms. The configuration of the hair strand is reconstructed from the generalized coordinates that conform to twist and curvature of the segments. This deformable model is by far the most advanced way to represent elastic rods. However, it has some important restrictions: Since the segments have an intrinsic curvature, the simulation of n-point contacts [vdHNGT03] or knots requires a large number of segments. As their approach has complexity $\mathcal{O}(N^2)$ with N the number of segments, such self-collision configurations can hardly be simulated at interactive rates. In contrast, our scheme is linear in the number of elements, and designed to handle complex contact configurations such as knots. Further, we replace the viscous dissipation energy of [BAC*06] by a term that additionally considers internal friction without affecting the rigid body motion of the rod.

The approaches that are most closely related to ours are the works of Grégoire et al. [GS06] and Loock et al. [LS01]. They proposed to model a cable from joined elements where each element has a position and an orientation, the latter expressed in terms of quaternions. Then they derive constraint energies and associated forces. The goal is to find static equilibria states of cables in virtual assembly simulation. We augment their work by considering the dynamics of rods, which provides unique challenges. Further, we employ finite element methods to derive discrete energies while they simulate the rod as a simple mass-spring system.

3. Cosserat theory of elastic rods

In this section, we give a brief introduction of the Cosserat theory of elastic rods. For a more comprehensive discussion of the topic, we refer to the book of Antman [Ant95].

3.1. Representation of rods

A rod can be thought of as a long and thin deformable body. We assume that its length is significantly larger than its radius, and thus we do not explicitly represent its volume. Instead, we characterize the continuous configuration of the rod by the *centerline* $\mathbf{r}(\sigma) = (r_x(\sigma), r_y(\sigma), r_z(\sigma))^\mathsf{T}$. Here, $\mathbf{r}(\sigma) : [0,1] \to \mathbb{R}^3$ assigns a position in space to each line parameter value $\sigma \in [0,1]$.

With this concept alone, we can not express the torsion of the rod. Thus, we think in each mass point of the rod a right-handed orthonormal basis $\mathbf{d}_1(\sigma), \mathbf{d}_2(\sigma), \mathbf{d}_3(\sigma)$. The $\mathbf{d}_i$ are called *directors*. $\mathbf{d}_3(\sigma)$ is defined to be tangential to the centerline, thus $\mathbf{d}_3$ is parallel to $\mathbf{r}'$:

$$\frac{\mathbf{r}'}{\|\mathbf{r}'\|} - \mathbf{d}_3 = 0 \qquad (1)$$

This important constraint realizes the mechanical coupling between the centerline and its orientation. Later, it will turn out that this constraint is not implicitly fulfilled but has to be explicitly enforced. Fig. 2 illustrates the representation of the rod. Notice that the prime $y'(\sigma, t)$ always denotes the spatial derivative $\frac{\partial y}{\partial \sigma}$, while the dot $\dot{y}(\sigma, t)$ denotes the temporal derivative $\frac{\partial y}{\partial t}$.
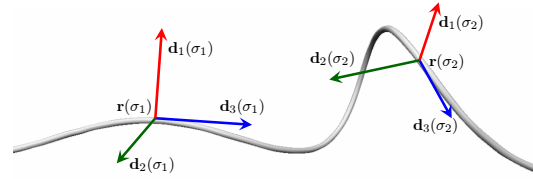
Figure 2: *The configuration of the rod is defined by its centerline $\mathbf{r}(\sigma)$. Further, the orientation of each mass point of the rod is represented by an orthonormal basis, called the directors. $\mathbf{d}_3(\sigma)$ is constrained to be parallel to $\mathbf{r}'(\sigma)$*

The length of the spatial derivative $\|\mathbf{r}'(\sigma)\|$ indicates the stretch of the centerline $\mathbf{r}$ at σ. Without loss of generality, we assume the length of the rod to be 1. As a consequence, $\|\mathbf{r}'\| = 1$ if the rod is unstretched. Some variants of the Cosserat rod model [MM96, BAC*06] consider the rod to be inextensible, which does, however, lead to stiff equations.

The spatial derivatives $\mathbf{d}'_k$ of the directors indicate the spatial rate of change in bending and torsion. From differential geometry, it is known that there exists a vector $\mathbf{u}$ with

$$\mathbf{d}'_k = \mathbf{u} \times \mathbf{d}_k, \qquad k = 1, 2, 3 \qquad (2)$$

$\mathbf{u}$ is called the *Darboux vector*. The Darboux vector is an important quantity in the Cosserat theory since the strain rates for the bending and torsion can be expressed as

$$u_k = \mathbf{u} \cdot \mathbf{d}_k, \qquad k = 1, 2, 3 \qquad (3)$$

The values u_1 and u_2 measure the strain in the two bending directions while u_3 measures the torsional strain. Later, we derive the expression for the potential energy from these strain rates.

The temporal derivative $\dot{\mathbf{r}}(\sigma)$ of the centerline indicates the translational velocity of the mass point at σ. The angular velocity ω is related to the temporal derivatives of the directors by

$$\dot{\mathbf{d}}_k = \omega \times \mathbf{d}_k, \qquad k = 1, 2, 3 \qquad (4)$$

The components $\omega_k = \omega \cdot \mathbf{d}_k$ measure the angular velocity of the cross section rotating around director $\mathbf{d}_k$.

3.2. Representation of rotation

In order to relate the directors $\mathbf{d}_i$ to the reference frame, we have to choose a representation of rotation, i. e. a representation for the group of orthogonal rotations SO(3). In the literature, both Euler angles, and quaternions (also known as Euler parameters) have been proposed.

The Euler angles use the minimum number of parameters to represent the rotation, but they suffer from singularities such as the gimbal lock. Having this in mind, we use quaternions to represent the rotation. A quaternion can be thought of as a quadruple $\mathbf{q} = (q_1, q_2, q_3, q_4)^\top$ with $q_i \in \mathbb{R}$. Only unit quaternions represent pure rotations, thus the q_i are not independent but coupled by the constraint $\|\mathbf{q}\| = 1$. The directors $\mathbf{d}_i$ in terms of the quaternion $\mathbf{q}$ are given by:

$$\mathbf{d}_1 = \begin{pmatrix} q_1^2 - q_2^2 - q_3^2 + q_4^2 \\ 2(q_1q_2 + q_3q_4) \\ 2(q_1q_3 - q_2q_4) \end{pmatrix}, \mathbf{d}_2 = \begin{pmatrix} 2(q_1q_2 - q_3q_4) \\ -q_1^2 + q_2^2 - q_3^2 + q_4^2 \\ 2(q_2q_3 + q_1q_4) \end{pmatrix}$$

$$\mathbf{d}_3 = \begin{pmatrix} 2(q_1q_3 + q_2q_4) \\ 2(q_2q_3 - q_1q_4) \\ -q_1^2 - q_2^2 + q_3^2 + q_4^2 \end{pmatrix} \quad (5)$$

The strain rates u_k in the local frame are obtained as

$$u_k = \frac{2}{\|\mathbf{q}\|^2} \mathbf{B}_k \mathbf{q} \cdot \mathbf{q}' \quad (6)$$

where $\mathbf{B}_k \in \mathbb{R}^{4 \times 4}$ is a constant skew-symmetric matrix. For the angular velocity components ω_k in the local frame, a similar relation is stated as

$$\omega_k = \frac{2}{\|\mathbf{q}\|^2} \mathbf{B}_k \mathbf{q} \cdot \dot{\mathbf{q}} \quad (7)$$

The angular velocity components ω_k^0 with respect to the reference frame are

$$\omega_k^0 = \frac{2}{\|\mathbf{q}\|^2} \mathbf{B}_k^0 \mathbf{q} \cdot \dot{\mathbf{q}} \quad (8)$$

where $\mathbf{B}_k^0 \in \mathbb{R}^{4 \times 4}$ is a constant skew-symmetric matrix. ω^0 is required to derive the angular dissipation energy. The derivation of (6) and (7) and the expressions for $\mathbf{B}_k$ and $\mathbf{B}_k^0$ are given in the Appendix.

3.3. Energy formulation

Based upon the strain-displacement and angular velocity relations (6), (7) and (8), we derive the continuous kinetic, potential and dissipation energy of the deformed rod.

3.3.1. Potential energy

The potential energy consists of two parts, namely the energy V_s of the stretch deformation, and the energy V_b of the bending and torsional deformation. The stretch energy V_s is given as

$$V_s = \frac{1}{2} \int_0^1 K_s(\|\mathbf{r}'\| - 1)^2 d\sigma \quad (9)$$

where shear is neglected. K_s is the stretching stiffness constant that is computed from a stretching Young's modulus

E_s with $K_s = E_s \pi r^2$. The bending energy V_b follows from the strain rates (6)

$$V_b = \frac{1}{2} \int_0^1 \sum_{k=1}^3 K_{kk}(\frac{2}{\|\mathbf{q}\|^2} \mathbf{B}_k \mathbf{q} \cdot \mathbf{q}' - \hat{u}_k)^2 d\sigma \quad (10)$$

The $\hat{u}_k$ conform to the intrinsic bending and torsion of the rod and $\mathbf{K} = (K_{kk}) \in \mathbb{R}^{3 \times 3}$ is the stiffness tensor. Since we assume that the rod has a uniform cross section, we can neglect the off-diagonal terms in $\mathbf{K}$. From textbooks on mechanics we get

$$K_{11} = K_{22} = E\frac{\pi r^2}{4}, \quad K_{33} = G\frac{\pi r^2}{2} \quad (11)$$

with E denoting the Young's modulus governing the bending resistance, G denoting the shear modulus governing the torsional resistance, and r denoting the radius of the rod's cross section.

For ideal rods, the stretching Young's modulus E_s is equal to the bending Young's modulus E. However, in order to get an additional degree of freedom, it is useful to define two independent constants E and E_s. This is motivated by the observation that e. g. nylon ropes do not have a uniform cross section, but are composed of several strands. As a consequence, the observed bending resistance is much lower than the theoretical bending resistance computed from the Young's modulus.

Together, we obtain the potential energy V as $V = V_s + V_b$. The values for r, E, E_s and G depend on the simulated material (see Appendix).

3.3.2. Kinetic energy

The kinetic energy of the rod consists of two parts, namely the translational energy T_t of the centerline $\mathbf{r}$, and the rotational energy T_r of the rod cross section. The translational energy is

$$T_t = \frac{1}{2} \int_0^1 \rho \pi r^2 \dot{\mathbf{r}} \cdot \dot{\mathbf{r}} d\sigma \quad (12)$$

where ρ is the density per unit length, and r is the radius of the rod. The rotational energy follows from the expressions for the angular velocities (7)

$$T_r = \frac{1}{2} \int_0^1 \sum_{k=1}^3 I_{kk}(\frac{2}{\|\mathbf{q}\|^2} \mathbf{B}_k \mathbf{q} \cdot \dot{\mathbf{q}})^2 d\sigma \quad (13)$$

where $\mathbf{I} = (I_{kk}) \in \mathbb{R}^{3 \times 3}$ is the inertia tensor that is approximated as

$$I_{11} = I_{22} = \rho\frac{\pi r^2}{4}, \quad I_{33} = \rho\frac{\pi r^2}{2} \quad (14)$$

As before, the off-diagonal terms in $\mathbf{I}$ can be neglected. The total kinetic energy T is then $T = T_t + T_r$. The numerical values for ρ and r are given in the Appendix.

3.3.3. Dissipation energy

The dissipation energy captures internal friction and visco-elastic effects. A heuristic model for visco-elastic effects has been proposed in [BAC*06]. To model internal friction, we propose an approach that is inspired by the pioneering work

of Baraff and Witkin [BW98] on constrained cloth simulation.

The internal friction damps relative velocity in the rod. The relative translational velocity can be computed as the spatial derivative of the temporal derivative of the centerline $\mathbf{r}$ acting in the tangential direction $\mathbf{r}'$. The translational dissipation energy D_t is

$$D_t = \frac{1}{2} \int_0^1 \gamma_t \mathbf{v}^{(rel)} \cdot \mathbf{v}^{(rel)} d\sigma \qquad (15)$$

where γ_t is the translational internal friction coefficient. $\mathbf{v}^{(rel)} = \frac{1}{\|\mathbf{r}'\|^2} \mathbf{r}'(\dot{\mathbf{r}}' \cdot \mathbf{r}')$ is the projected relative translational velocity of the mass points.

The relative angular velocity is obtained from the spatial derivative of the angular velocity ω_0. It is important to compute the angular velocity in the reference frame in order to consider all quantities in the same basis. The rotational dissipation energy D_r is then

$$D_r = \frac{1}{2} \int_0^1 \gamma_r \omega_0' \cdot \omega_0' d\sigma \qquad (16)$$

where γ_r is the rotational internal friction coefficient. ω_0 can be obtained from (8). The total dissipation energy $D = D_t + D_r$ is the sum of the translational and rotational dissipation energy.

3.4. Lagrangian equation of motion

The dynamic equilibrium configuration of an elastic rod is characterized as a critical point of the Lagrangian $L = T - V + D$ subject to the holonomic constraints

$$\mathbf{C}_p \equiv \frac{\mathbf{r}'}{\|\mathbf{r}'\|} - \mathbf{d}_3 = 0 \qquad (17)$$

$$C_q \equiv \|\mathbf{q}\|^2 - 1 = 0 \qquad (18)$$

The vector-valued constraint (17) states that the third director conforms to the spatial derivative of the centerline $\mathbf{r}$. This constraint couples the orientations and the positions of the rod. The scalar constraint (18) states that the quaternion has unit length and thus represents a proper rotation.

By employing calculus of variations and by introducing Lagrangian multipliers $\lambda \in \mathbb{R}^3$ and $\mu \in \mathbb{R}$ for the constraints, we obtain the Lagrangian equation of motion for an elastic rod:

$$\frac{d}{dt}\frac{\partial T}{\partial \dot{g}_i} - \frac{\partial T}{\partial g_i} + \frac{\partial V}{\partial g_i} + \frac{\partial D}{\partial \dot{g}_i} + \lambda \cdot \frac{\partial \mathbf{C}_p}{\partial g_i} + \mu \frac{\partial C_q}{\partial g_i} = \int_0^1 \mathbf{F}_e d\sigma \qquad (19)$$

Here, the $g_i \in \{r_x, r_y, r_z, q_1, q_2, q_3, q_4\}$ are the coordinates, and $\mathbf{F}_e$ are external forces and torques. Details can be found in the book of Goldstein [Gol81].

4. Discrete energy formulation

In this section, we discretize the rod into elements. We then derive expressions for the potential and kinetic energy per element by employing finite element methods. This discretization allows for an efficient numerical solution of the equations of motion (19).

4.1. Discretization of the rod

We represent the centerline $\mathbf{r}(\sigma)$ of the rod as a chain of N nodes $\mathbf{r}_i \in \mathbb{R}^3, i \in [1,N]$. The centerline elements $\mathbf{r}_{i+1} - \mathbf{r}_i$ may differ in size. The orientations of the centerline elements are represented by quaternions $\mathbf{q}_j, j \in [1, N-1]$, as illustrated in Fig. 3. A similar representation has been proposed by Grégoire and Schömer in [GS06]. In contrast to pure geometric approaches such as [LMGC02], this representation allows to model material torsion.
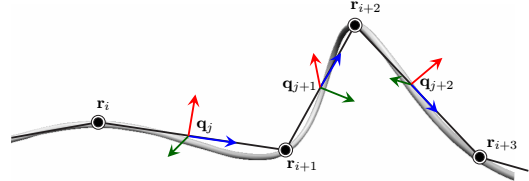
Figure 3: *The centerline of the rod is discretized into nodes* $\mathbf{r}_i$. *The orientation of the centerline element* $\mathbf{r}_{i+1} - \mathbf{r}_i$ *is represented by a quaternion* $\mathbf{q}_j$ *that is attached to the centerline element at its midpoint.*

The discrete spatial derivative $\mathbf{r}_i'$ of the centerline is obtained as $\mathbf{r}_i' = \frac{\mathbf{r}_{i+1} - \mathbf{r}_i}{\|\mathbf{r}_{i+1} - \mathbf{r}_i\|}$. By assuming a high stretch stiffness, we approximate $\mathbf{r}_i'$ as

$$\mathbf{r}_i' \approx \frac{1}{l_i}(\mathbf{r}_{i+1} - \mathbf{r}_i) \qquad (20)$$

where $l_i = \|\mathbf{r}_{i+1}^0 - \mathbf{r}_i^0\|$ is the resting length of the centerline element i. Here, the $\mathbf{r}_i^0$ are the initial positions of the mass points.

To derive an expression for the discrete spatial derivative $\mathbf{q}_j'$ of the orientation, we consider that the quaternion $\mathbf{q}_j$ represents the orientation of the centerline element $\mathbf{r}_{i+1} - \mathbf{r}_i$. Thus, an orientation element j starts at the midpoint of centerline element i and ends at the midpoint of centerline element $i + 1$. For $\mathbf{q}_j'$, we thus approximate

$$\mathbf{q}_j' \approx \frac{1}{l_j}(\mathbf{q}_{j+1} - \mathbf{q}_j) \qquad (21)$$

where $l_j = \frac{1}{2}(\|\mathbf{r}_{i+2}^0 - \mathbf{r}_{i+1}^0\| + \|\mathbf{r}_{i+1}^0 - \mathbf{r}_i^0\|)$ is the resting length of the orientation element j.

4.2. Discrete energies

In this section, we derive the formulations of the potential, kinetic and dissipation energy for the discrete Cosserat rod. We compute the energies per centerline and orientation element by integrating the energies over the length of the respective element. The total energy of the rod could then be obtained by summing up the individual energies. However, this will not be necessary since we solve the Lagrangian equation of motion per node.

In our discrete setting, the displacements are only given at the nodes. Therefore, we interpolate the displacements

within the elements. For simplicity, we employ constant shape functions $\bar{\mathbf{r}}(\xi)$ and $\bar{\mathbf{q}}(\xi)$, i. e.

$$\bar{\mathbf{r}}_i(\xi) = \bar{\mathbf{r}}_i = \frac{1}{2}(\mathbf{r}_i + \mathbf{r}_{i+1}) \qquad (22)$$

and

$$\bar{\mathbf{q}}_j(\xi) = \bar{\mathbf{q}}_j = \frac{1}{2}(\mathbf{q}_j + \mathbf{q}_{j+1}) \qquad (23)$$

These shape functions result in particularly simple expressions when integrated over the element length. Experiments indicate that higher-order shape functions do barely increase the visual plausibility, but require significantly more computations.

4.2.1. Discrete potential energy

To derive the expression for the stretch energy, we integrate over the length l_i of the centerline segment i. Assuming that the spatial derivative $\mathbf{r}'_i$ stays constant per element, the stretch energy per element i follows from (9) as

$$
\begin{aligned}
V_s[i] &= \frac{1}{2}\int_0^{l_i} K_s(\|\mathbf{r}'_i\| - 1)^2 d\xi \\
&= \frac{1}{2}l_i K_s\left(\frac{1}{l_i}\sqrt{(\mathbf{r}_{i+1}-\mathbf{r}_i)\cdot(\mathbf{r}_{i+1}-\mathbf{r}_i)} - 1\right)^2 \quad (24)
\end{aligned}
$$

To derive the expression for the bending energy, we integrate over the length l_j of the orientation element j. We further assume that the spatial derivative $\mathbf{q}'_j$ stays constant. Thus

$$
\begin{aligned}
V_b[j] &= \frac{1}{2}\int_0^{l_j}\sum_{k=1}^{3} K_{kk}\left(\underbrace{\frac{2}{\|\bar{\mathbf{q}}_j\|^2}}_{\approx 2}\mathbf{B}_k\bar{\mathbf{q}}_j\cdot\mathbf{q}'_j - \hat{u}_k\right)^2 d\xi \quad (25) \\
&= \frac{l_j}{2}\sum_{k=1}^{3} K_{kk}\left(\mathbf{B}_k(\mathbf{q}_j + \mathbf{q}_{j+1})\cdot\frac{1}{l_j}(\mathbf{q}_{j+1} - \mathbf{q}_j) - \hat{u}_k\right)^2
\end{aligned}
$$

where we made the simplifying assumption that the quaternions have unit length, which is justified since the unit-constraint (18) is explicitly enforced.

4.2.2. Discrete kinetic energy

Similar to the previous section, we consider the kinetic translational energy per centerline element, and the kinetic rotational energy per orientation element. By plugging (22) into (12) and integrating over the centerline element i, we get

$$
\begin{aligned}
T_t[i] &= \frac{1}{2}\int_0^{l_i}\rho\pi r^2 \dot{\mathbf{r}}_i\cdot\dot{\mathbf{r}}_i d\xi \\
&= \frac{1}{8}\rho\pi r^2 l_i(\dot{\mathbf{r}}_{i+1}+\dot{\mathbf{r}}_i)\cdot(\dot{\mathbf{r}}_{i+1}+\dot{\mathbf{r}}_i) \quad (26)
\end{aligned}
$$

For the rotational kinetic energy, we integrate over the orientation element j. The resulting energy expression is

$$
\begin{aligned}
T_r[j] &= \frac{1}{2}\int_0^{l_j}\sum_{k=1}^{3} I_{kk}\left(\underbrace{\frac{2}{\|\bar{\mathbf{q}}_j\|^2}}_{\approx 2}\mathbf{B}_k\bar{\mathbf{q}}_j\cdot\dot{\mathbf{q}}_j\right)^2 d\xi \\
&= \frac{l_j}{8}\sum_{k=1}^{3} I_{kk}\left(\mathbf{B}_k(\mathbf{q}_j + \mathbf{q}_{j+1})\cdot(\dot{\mathbf{q}}_j + \dot{\mathbf{q}}_{j+1})\right)^2 \quad (27)
\end{aligned}
$$

4.2.3. Discrete dissipation energy

To obtain the dissipation energy expression, we proceed as in the previous sections. Again, the translational dissipation energy is obtained by integrating over the centerline elements, and the rotational dissipation energy is obtained by integrating over the orientation elements. For the translational dissipation energy D_t we get

$$
\begin{aligned}
D_t[i] &= \frac{1}{2}\int_0^{l_i}\gamma_t\mathbf{v}_i^{(rel)}\cdot\mathbf{v}_i^{(rel)} d\xi \\
&= \frac{l_i}{2}\gamma_t\mathbf{v}_i^{(rel)}\cdot\mathbf{v}_i^{(rel)} \quad (28)
\end{aligned}
$$

with the projected relative translational velocity $\mathbf{v}_i^{(rel)}$ as

$$
\begin{aligned}
\mathbf{v}_i^{(rel)} &= \underbrace{\frac{1}{\|\mathbf{r}'_i\|^2}}_{\approx 1}\mathbf{r}'_i(\dot{\mathbf{r}}'_i\cdot\mathbf{r}'_i) \\
&= \frac{1}{l_i^3}(\mathbf{r}_{i+1}-\mathbf{r}_i)\left((\dot{\mathbf{r}}_{i+1}-\dot{\mathbf{r}}_i)\cdot(\mathbf{r}_{i+1}-\mathbf{r}_i)\right) \quad (29)
\end{aligned}
$$

where we made the simplifying assumption that $\|\mathbf{r}'_i\| \approx 1$, which is valid for rods with a large stretching stiffness. The rotational dissipation energy D_r is obtained as

$$
\begin{aligned}
D_r[j] &= \frac{1}{2}\int_0^{l_j}\gamma_r\sum_{k=1}^{3}\left(\frac{1}{l_j}2\mathbf{B}_k^0\mathbf{q}_{j+1}\dot{\mathbf{q}}_{j+1} - \frac{1}{l_j}2\mathbf{B}_k^0\mathbf{q}_j\dot{\mathbf{q}}_j\right)^2 d\xi \\
&= \frac{2}{l_j}\gamma_r\sum_{k=1}^{3}\left(\mathbf{B}_k^0\mathbf{q}_{j+1}\dot{\mathbf{q}}_{j+1} - \mathbf{B}_k^0\mathbf{q}_j\dot{\mathbf{q}}_j\right)^2 \quad (30)
\end{aligned}
$$

where we assume $\|\mathbf{q}_j\| \approx 1$ for all j. Notice that here we do not interpolate the displacements within the orientation element but compute the relative rotational velocity between the two orientation nodes. It is important to take the relative velocities with respect to the reference frame.

5. Numerical solution

In the last section, we have divided the rod into elements. For each element, we have derived the potential, kinetic and dissipation energy. We now show how we can solve the Lagrangian equation of motion by employing those energy terms. We further propose an efficient implementation of the necessary constraints such that the system of equations is decoupled.

5.1. Assembly of the equations of motion

The Lagrangian equation of motion (19) characterizes the dynamic equilibrium of the rod. By substituting the continuous energies in (19) with the per-element energies derived in the previous section, we arrive at the discrete Lagrangian equation of motion that characterizes the dynamic equilibrium per element. The necessary symbolic differentiation is performed by employing the computer algebra software Maple. This results in a system of equations of the form

$$\mathbf{M}\ddot{\mathbf{g}} + \mathbf{f}(\dot{\mathbf{g}}, \mathbf{g}) = (\mathbf{F}_e\ \tau_e)^\top \qquad (31)$$

The matrix $\mathbf{M}(\dot{\mathbf{g}}, \mathbf{g})$ contains nonlinear terms in $\dot{\mathbf{g}} = \{\dot{\mathbf{r}}, \dot{\mathbf{q}}\}$ and $\mathbf{g} = \{\mathbf{r}, \mathbf{q}\}$. Further, $\mathbf{f}(\dot{\mathbf{g}}, \mathbf{g})$ conforms to a nonlinear stiffness function that is obtained by symbolically differentiating

the potential and dissipation energy with respect to the co-ordinates. Evaluating this function results in internal forces and torques. $\mathbf{F}_e$ and τ_e are the external forces and torques that act on the rod.

The system of equations can be solved by employing iterative methods, e. g. with a conjugate gradient method. However, the numerical solution is expensive and can hardly be done at interactive rates for larger rods. In the next two sections, we propose two simplifications of the problem that result in a decoupled system of equations that can be solved directly.

5.2. Implementation of the constraints

The coupling between the orientation of the rod and its centerline is realized by the constraint (17). To implement the constraints in (19), we have introduced Lagrangian multipliers.

At this point, we underline that a Cosserat rod is an intrinsically constrained system. In computer graphics, many approaches have been presented on maintaining constraints in dynamic systems. An application of Lagrangian multipliers to articulated rigid bodies has e. g. been proposed by Baraff [Bar96]. Earlier, Witkin et al. [WFB87] have proposed to express geometric constraints by energy functions, an approach that is also known as *penalty method*. They formulated a constraint as an energy function $E(\mathbf{x}) : \mathbb{R}^n \to \mathbb{R}$ with $E(\mathbf{x}) = 0$ if the constraint is satisfied. Differentiating this energy function with respect to $\mathbf{x}$ yields constraint forces $\mathbf{F}$ that accelerate the system towards the desired configuration.

The advantage of the penalty method is its efficiency: The constraints do not appear as additional equations in the Lagrangian equation of motion, but they act as additional forces on the system. The disadvantage is the loss of physical accuracy: Since the constraint forces act during a time period h on the system, they violate the principle of virtual power [Gol81]. However, since our goal is to obtain a simulation that behaves in a physical plausible way, we decided to employ energy constraints. We thus express the parallel constraint (17) by an energy function

$$E_p = \frac{1}{2} \int_0^1 \kappa \left(\frac{\mathbf{r}'}{\|\mathbf{r}'\|} - \mathbf{d}_3 \right) \cdot \left(\frac{\mathbf{r}'}{\|\mathbf{r}'\|} - \mathbf{d}_3 \right) d\sigma \quad (32)$$

where κ is a spring constant. In our discrete model, the direction of the centerline element $\mathbf{r}_{i+1} - \mathbf{r}_i$ has to conform to the third director of the basis representing the orientation of this element. Thus, the discrete constraint energy per centerline element reads as

$$\begin{aligned} E_p[i] &= \frac{1}{2} \int_0^{l_i} \kappa \left(\frac{\mathbf{r}_i'}{\|\mathbf{r}_i'\|} - \mathbf{d}_3(\mathbf{q}_i) \right) \cdot \left(\frac{\mathbf{r}_i'}{\|\mathbf{r}_i'\|} - \mathbf{d}_3(\mathbf{q}_i) \right) d\xi \quad (33) \\ &= \frac{l_i}{2} \kappa \left(\frac{\mathbf{r}_{i+1} - \mathbf{r}_i}{\|\mathbf{r}_{i+1} - \mathbf{r}_i\|} - \mathbf{d}_3(\mathbf{q}_i) \right) \cdot \left(\frac{\mathbf{r}_{i+1} - \mathbf{r}_i}{\|\mathbf{r}_{i+1} - \mathbf{r}_i\|} - \mathbf{d}_3(\mathbf{q}_i) \right) \end{aligned}$$

What have we gained with this constraint transformation? The constraint energy $E_p[i]$ can now be treated as an additional potential energy term in the Lagrangian equation of motion of the rod. By symbolic differentiation, we obtain an additional internal force term acting on the mass points and an additional internal torque term acting on the quaternions. In fact, these forces and torques are responsible for

many rod phenomena such as buckling and looping. The numerical values of κ depend on the simulated material (see Appendix).

To enforce the quaternion unit length constraint (18), we employ an even simpler method that is sometimes referred as coordinate projection [ESF98]: In each iteration of the numerical simulation, we explicitly renormalize the quaternions $\hat{\mathbf{q}}_i$, i. e. $\mathbf{q}_i \leftarrow \frac{\hat{\mathbf{q}}_i}{\|\hat{\mathbf{q}}_i\|}$. Although this technique does not guarantee energy conservation, it does not harm the visual quality of the simulation.

5.3. Decoupling of the state equations

By expressing the constraint (17) by an energy function, we have reduced the number of equations in (31). The accelerations $\ddot{\mathbf{q}}$ and $\ddot{\mathbf{r}}$ are obtained by inverting the mass matrix $\mathbf{M}$. This is accomplished by considering the structure of $\mathbf{M}$. Since the positions and orientations are exclusively coupled by the constraint energy, $\mathbf{M}$ has a block-diagonal form

$$\mathbf{M} = \begin{pmatrix} \mathbf{M}_r & \mathbf{0} \\ \mathbf{0} & \mathbf{M}_q \end{pmatrix} \quad (34)$$

where $\mathbf{M}_r$ is the mass matrix governing the state equations of the mass points $\mathbf{r}_i$, and $\mathbf{M}_q$ is the mass matrix of the quaternions $\mathbf{q}_j$.

Since we assume that the mass is lumped in the mass points $\mathbf{r}_i$, the mass matrix $\mathbf{M}_r$ is diagonal. The equations of motion for the mass points are obtained as

$$\begin{aligned} \dot{\mathbf{v}}_i &= \frac{\mathbf{F}_i}{m_i} \\ \dot{\mathbf{r}}_i &= \mathbf{v}_i \end{aligned} \quad (35)$$

where $\mathbf{F}_i$ is the sum of internal and external forces acting on the mass point, $\mathbf{v}_i$ its velocity, and m_i its mass.

The mass matrix $\mathbf{M}_q$ governing the evolution of the quaternions is not diagonal. However, it is possible to express the equations of motion not by the quaternions and their time derivatives, but to use the angular velocities ω_j together with the quaternions $\mathbf{q}_j$ as state variables [SM06]. This results in a diagonalized system of equations for the quaternions,

$$\begin{aligned} \dot{\omega}_j &= \mathbf{I}^{-1}(\tau_j - \omega_j \times \mathbf{I}\omega_j) \\ \dot{\mathbf{q}}_j &= \frac{1}{2} \mathbf{Q}_j \begin{pmatrix} 0 \\ \omega_j \end{pmatrix} \end{aligned} \quad (36)$$

Here, τ_j is the sum of internal and external torques that act on the quaternion, $\mathbf{I}$ is the inertia tensor, and $\mathbf{Q}_j$ is the quaternion matrix of $\mathbf{q}_j$. The quaternion matrix allows to write a quaternion multiplication as a matrix-vector product,

(35) and (36) define an initial value problem (IVP), where the initial configuration of the rod is user-defined. The IVP is solved by numerical integration, as discussed in the subsequent section.

5.4. Numerical solution of the initial value problem

We summarize the simulation process. The stiffness function $\mathbf{f}(\dot{\mathbf{r}}, \mathbf{r}, \dot{\mathbf{q}}, \mathbf{q})$ that governs the computation of the internal forces and torques is obtained by differentiating the potential and constraint energy with respect to the coordinates $\mathbf{r}$ and

q, and by differentiating the dissipation energy with respect to the time derivatives $\dot{\mathbf{r}}$ and $\dot{\mathbf{q}}$. This symbolic differentiation is done as a preprocessing step.

Subsequent positions $\mathbf{r}^{t+h}$ and orientations $\mathbf{q}^{t+h}$ are obtained by time integration of the state equations (35) and (36). The internal forces and torques are obtained from evaluating $\mathbf{f}(\dot{\mathbf{r}}^t, \mathbf{r}^t, \dot{\mathbf{q}}^t, \mathbf{q}^t)$ in the current configuration of the rod. External forces include gravity, contact forces, and user interactions. External torques are neglected. We denote the resulting sum of internal and external forces in the current configuration as $\mathbf{F}^t$ and the resulting internal torques as τ^t.

To evolve the mass points, we numerically integrate the state equations (35) by employing a semi-implicit Euler scheme:

$$\mathbf{v}_i^{t+h} = \mathbf{v}_i^t + \frac{h}{m_i}\mathbf{F}^t \tag{37}$$

$$\mathbf{r}_i^{t+h} = \mathbf{r}_i^t + h\mathbf{v}_i^{t+h} \tag{38}$$

This scheme provides sufficient conditional stability at minor computational overhead.

The evolution of the orientations is slightly more involved. The torques $\tau^t \in \mathbb{R}^4$ resulting from evaluating **f** are dual to the quaternions. However, to evolve the angular velocities ω, we need to transform the τ^t into Euclidean torques $\tilde{\tau}^t \in \mathbb{R}^3$. This transformation is accomplished by a multiplication with the transposed quaternion matrix,

$$\begin{pmatrix} 0 \\ \tilde{\tau}_j \end{pmatrix} = \frac{1}{2}\mathbf{Q}_j^{\mathsf{T}}\tau_j \tag{39}$$

For details on quaternion transformations we refer to Schwab and Meijaard [SM06]. The numerical integration of the rotational state equations (36) is also realized with the semi-implicit Euler scheme,

$$\omega_j^{t+h} = \mathbf{I}^{-1}(\tilde{\tau}_j^t - \omega_j^t \times (\mathbf{I}\omega_j^t))h + \omega_j^t \tag{40}$$

$$\hat{\mathbf{q}}_j^{t+h} = \frac{1}{2}\mathbf{Q}_j^t\begin{pmatrix} 0 \\ \omega_j^{t+h} \end{pmatrix}h + \mathbf{q}_j^t \tag{41}$$

$$\mathbf{q}_j^{t+h} = \frac{\hat{\mathbf{q}}_j^{t+h}}{\|\hat{\mathbf{q}}_j^{t+h}\|} \tag{42}$$

where the last step explicitly normalizes the quaternions.

6. Results

The purpose of the experiments is to illustrate the physical plausibility of our deformation model. Further, we show that the approach is well-suited for interactive applications.

To enable contact and self-contact configurations, we have implemented a standard deformable model collision handling scheme [TKH*05]. To detect collisions, we employ axis-aligned bounding box hierarchies, and to compute the repulsion forces, we employ an adaptation of the constraint-based response scheme from [SBT07]. All experiments have been staged on an Intel Xeon PC, 3.8GHz. The offline rendering is accomplished with a raytracer, the real-time rendering with OpenGL. For rendering, the rods are skinned with a tubical, B-spline interpolated surface mesh.

# Elements	Force comp. [ms]	Integration [ms]
50	0.051	0.018
100	0.096	0.035
1000	0.91	0.33

Table 1: *Timings for the force computation and integration of discretized rods. The timings indicate that the method is linear in the number of elements.*

6.1. Discrete rods

The purpose of these experiments is to show that the dynamic global behavior of real rods can be reproduced. The material parameters are summarized in Tab. 2 in the Appendix.

In a first experiment, we study the global deformation of clamped rods that occur when the end-to-end rotation is varied. These experiments are inspired by recent research in the field of nonlinear mechanics [vdHNGT03]. The experimental setup is shown in Fig. 1 on the left. A torque transducer exerts a continued torsional rotation on the rod, while the right end of the rod stays clamped. The rod forms a looping with an increasing number of self-contacts. The number of self-contacts is obviously limited by the number of elements of the rod. The radius and the location of the loop are influenced by the ratio of bending and torsion stiffness [vdHNGT03]. The time step of the simulation is $h = 0.1$ms. The rod is discretized into 100 elements. To validate our deformation model, we performed the same experiment with a real rope. Fig. 4 illustrates the looping sequence of the rope under torsional strain. Although the material parameters of the real rope differ in magnitude, its global deformation is comparable to the simulated virtual rope.
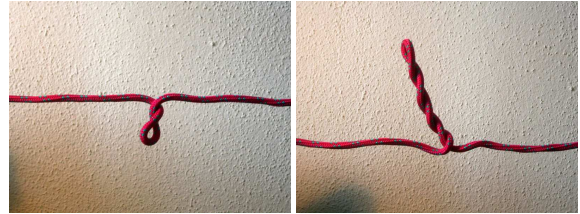
Figure 4: *To validate our deformation model, we performed the varied end-to-end rotation experiment with a real rope. The global deformation is comparable to the simulated virtual rope in Fig. 1.*

Figure 5: *Coiling up three clamped rods. The rods are discretized into 1000, 100 and 50 elements, illustrating that the global deformation is independent of the discretization.*

In a second experiment, we clamp the left ends of three rods to torque transducers. The transducers exert a continued rotation on the rods, thus coiling up the rods (see Fig. 5). The front rod is discretized into 1000 elements, the middle rod is discretized into 100 elements and the back rod is discretized into 50 elements. The time step is $h = 0.1$ms. The figures illustrate that the global deformation of the rods is independent of the discretization. Further, this experiment illustrates that our deformation model is linear in the number of elements. Timings are summarized in Tab. 1.

6.2. Pre-shaped stiff objects

Due to the robustness of our deformation model, a broad variety of different materials can be simulated. We can simulate highly flexible structures such as ropes as well as stiff objects such as bars. By defining an intrinsic bending and torsion, it is also possible to simulate pre-shaped objects such as springs. In these experiments, we model stiff wire-like objects whose material parameters are summarized in Tab. 2 in the Appendix. Each rod is discretized into 50 elements. The stiff equations require a small time step $h = 0.05$ms. Fig. 6 illustrates the dynamic simulations.
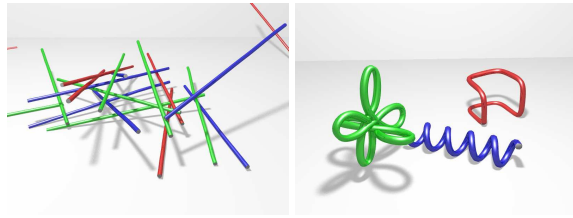
Figure 6: *Dynamic simulation of stiff objects. Left: Stacking of rods. Right: Objects with intrinsic bending and torsion.*

6.3. Virtual interactive ropes and threads

Since our approach is linear in the number of elements, elastic rods can be simulated at interactive rates. Further, internal friction minimizes oscillations and makes the material look more realistic.

To illustrate that our deformation model can be used in interactive applications, we run a simulation of a thread consisting of 100 elements. Its material parameters are summarized in Tab. 2 in the Appendix. While one end of the thread is clamped, the user can freely interact with the centerline (Fig. 7). In this experiment, the user ties a knot into the thread. The time step is $h = 2$ms, and the configuration is rendered after 20 simulation steps. The simulation runs at 26 frames per second. As indicated in Fig. 7 on the bottom right, it is also possible to interact with an intrinsically coiled thread.

7. Conclusion and future work

We have presented CORDE, a physically-based deformation model to simulate one-dimensional elastic objects. The deformation model is inspired by the Cosserat theory of elastic rods. We have discretized the rod into elements. For each element, we have derived the Lagrange equations
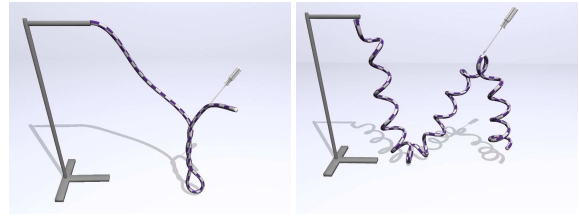
Figure 7: *Interactive simulation of threads. The user can freely interact with the thread. Oscillations are minimized by modeling internal friction.*

of motion by employing finite element methods. By numerically integrating these equations, the rod is evolved in time. In contrast to previous mass-spring approaches, the rod behavior is independent of the underlying discretization, and the finite element approach enables physically plausible simulation. In contrast to previous boundary value approaches [Pai02, BAC*06], the nodal approach allows for accurate and efficient collision and self-collision handling.

By employing our deformation model, a broad variety of different materials can be plausibly simulated and animated. This is partially enabled by modeling internal friction such that the rigid body motion of the rod is not affected. Since our method is linear in the number of nodes, the approach is particularly interesting for interactive applications. Moreover, the approach is elegant and simple to implement.

However, this deformation model is just a starting point for future research. In order to improve the physical accuracy of the method, a constraint handling that considers the principle of virtual power would be favorable. Since the constraint couples positions and orientations, this is a challenging problem. Further, virtual suturing requires that the thread can be tied to tight knots, which requires a solid collision handling. Currently, we are investigating into improved collision detection and response methods. Since the elements may differ in size, the rod can be adaptively refined in regions where precise collision handling is necessary.

References

[Ant95] ANTMAN S. S.: *Nonlinear Problems of Elasticity*. Springer Verlag, 1995.

[BAC*06] BERTAILS F., AUDOLY B., CANI M.-P., QUERLEUX B., LEROY F., LÉVÊQUE J.-L.: Super-helices for predicting the dynamics of natural hair. In *ACM Transactions on Graphics (Proc. SIGGRAPH)* (2006), pp. 1180–1187.

[Bar96] BARAFF D.: Linear-time dynamics using lagrange multipliers. *Computer Graphics (Proc. SIGGRAPH)* (1996), 137–146.

[BLM04] BROWN J., LATOMBE J.-C., MONTGOMERY K.: Real-time knot tying simulation. *The Visual Computer 20*, 2–3 (2004), 165–179.

[BW98] BARAFF D., WITKIN A.: Large steps in cloth simulation. In *Proc. SIGGRAPH* (1998), pp. 43–54.

[CJY02] CHANG J. T., JIN J., YU Y.: A practical model for hair mutual interactions. In *Proc. ACM SIGGRAPH/Eurographics symposium on Computer animation* (2002), pp. 73–80.

[CLW06] CAO D. Q., LIU D., WANG C. H.-T.: Three dimensional nonlinear dynamics of slender structures: Cosserat rod element approach. *International Journal of Solids and Structures 43*, 3–4 (2006), 760–783.

[Dic94] DICHMANN D. J.: *Hamiltonian Dynamics of a Spatial Elastica and the Stability of Solitary Waves*. PhD thesis, 1994. University of Maryland.

[ESF98] EICH-SOELLNER E., FÜHRER C.: *Numerical methods in multibody dynamics*. European Consortium for Mathematics in Industry. B. G. Teubner, Stuttgart, 1998.

[Gol81] GOLDSTEIN H.: *Classical Mechanics*, 2 ed. Addison-Wesley, 1981.

[GS06] GRÉGOIRE M., SCHÖMER E.: Interactive simulation of one-dimensional flexible parts. In *Proc. ACM Symposium on Solid and physical modeling* (2006), pp. 95–103.

[Had06] HADAP S.: Oriented strands: dynamics of stiff multi-body system. In *Proc. ACM SIGGRAPH/Eurographics symposium on Computer animation* (2006), pp. 91–100.

[Keh97] KEHRBAUM S.: *Hamiltonian Formulations of the Equilibrium Conditions Governing Elastic Rods: Qualitative Analysis and Effective Properties*. PhD thesis, 1997. University of Maryland.

[LMGC02] LENOIR J., MESEURE P., GRISONI L., CHAILLOU C.: Surgical thread simulation. *Modelling & Simulation for Computer-aided Medicine and Surgery* (2002), 102–107.

[LS01] LOOCK A., SCHÖMER E.: A virtual environment for interactive assembly simulation: From rigid bodies to deformable cables. In *Proc. 5th World Multiconference on Systemics, Cybernetics and Informatics* (2001), vol. 3, pp. 325–332.

[MG04] MÜLLER M., GROSS M.: Interactive virtual materials. In *Proc. Graphics interface* (2004), pp. 239–246.

[MM96] MANNING R. S., MADDOCKS J. H.: A continuum rod model of sequence-dependent dna structure. *J. Chem. Phys. 105* (1996), 5626–5646.

[NMK*05] NEALEN A., MÜLLER M., KEISER R., BOXERMANN E., CARLSON M.: Physically Based Deformable Models in Computer Graphics. In *Eurographics-STAR* (2005), pp. 71–94.

[Pai02] PAI D.: Strands: Interactive simulation of thin solids using cosserat models. *Computer Graphics Forum (Eurographics) 21*, 3 (2002), 347–352.

[PLK02] PHILLIPS J., LADD A., KAVRAKI L. E.: Simulated knot tying. In *Proc. IEEE International Conference on Robotics & Automation* (2002), pp. 841–846.

[QT96] QIN H., TERZOPOULOS D.: D-NURBS: A Physics-Based Framework for Geometric Design. *IEEE Transactions on Visualization and Computer Graphics 2*, 1 (1996), 85–96.

[RNG00] REMION Y., NOURRIT J.-M., GILLARD D.: A dynamic animation engine for generic spline objects. *Journal of Visualization and Computer Animation 11*, 1 (2000), 17–26.

[SBT07] SPILLMANN J., BECKER M., TESCHNER M.: Non-iterative computation of contact forces for deformable objects. *Journal of WSCG 15*, 1-3 (2007), 33–40.

[Sim85] SIMO J. C.: A finite strain beam formulation. the three-dimensional dynamic problem. part I. *Computer Methods in Applied Mechanics and Engineering 49* (1985), 55–70.

[SM06] SCHWAB A. L., MEIJAARD J. P.: How to draw euler angles and utilize euler parameters. In *Proc. IDETC/CIE 2006, ASME 2006 International Design Engineering Technical Conferences & Computers and Information in Engineering Conference* (2006).

[TKH*05] TESCHNER M., KIMMERLE S., HEIDELBERGER B., ZACHMANN G., RAGHUPATHI L., FUHRMANN A., CANI M.-P., FAURE F., MAGNENAT-THALMANN N., STRASSER W., VOLINO P.: Collision Detection for Deformable Objects. *Computer Graphics Forum 24*, 1 (2005), 61–81.

[TPBF87] TERZOPOULOS D., PLATT J., BARR A., FLEISCHER K.: Elastically deformable models. *Computer Graphics (Proc. SIGGRAPH) 21*, 4 (1987), 205–214.

[vdHNGT03] VAN DER HEIJDEN G., NEUKIRCH S., GOSS V., THOMPSON J.: Instability and self-contact phenomena in the writhing of clamped rods. *International Journal of Mechanical Sciences 45*, 1 (2003), 161–196.

[WBD*05] WANG F., BURDET E., DHANIK A., POSTON T., TEO C.: Dynamic thread for real-time knot-tying. In *Proc. First Joint Eurohaptics Conference and Symposium on Haptic Interfaces for Virtual Environment and Teleoperator Systems* (2005), pp. 507–508.

[WFB87] WITKIN A., FLEISCHER K., BARR A.: Energy constraints on parameterized models. *Computer Graphics 21*, 4 (1987), 225–232.

Appendix A: Derivation of strain rates in terms of quaternions

In this section, we derive the expression (6) that relates the strain rates u_k to the quaternions $\mathbf{q}$. The derivation of the relation between the angular velocity ω and the quaternions $\mathbf{q}$ is similar. The construction is a summary from the corresponding issue in the thesis of Dichmann [Dic94]. For further details, we refer the reader to the cited document.

We know that there exists the Darboux vector $\mathbf{u}$ that is related to the directors $\mathbf{d}_k$ by

$$\mathbf{d}_k' = \mathbf{u} \times \mathbf{d}_k, \qquad k = 1, 2, 3 \tag{43}$$

where the components u_k of $\mathbf{u}$ are directly proportional to the strain rates. Since the $\mathbf{d}_k$ define an orthonormal basis, we write $\mathbf{u} = u_1 \mathbf{d}_1 + u_2 \mathbf{d}_2 + u_3 \mathbf{d}_3$. For $\mathbf{d}_3'$, we then obtain for example

$$\begin{aligned} \mathbf{d}_3' &= (u_1 \mathbf{d}_1 + u_2 \mathbf{d}_2 + u_3 \mathbf{d}_3) \times \mathbf{d}_3 \\ &= u_1 \mathbf{d}_1 \times \mathbf{d}_3 + u_2 \mathbf{d}_2 \times \mathbf{d}_3 + u_3 \mathbf{d}_3 \times \mathbf{d}_3 \\ &= -u_1 \mathbf{d}_2 + u_2 \mathbf{d}_1 \end{aligned} \tag{44}$$

where we used the identities $\mathbf{d}_3 = \mathbf{d}_1 \times \mathbf{d}_2$ and $\mathbf{d}_k \times \mathbf{d}_k = 0, k = 1, 2, 3$. Multiplying (44) by $-\mathbf{d}_2$ yields

$$-\mathbf{d}_2 \cdot \mathbf{d}_3' = u_1 \mathbf{d}_2 \cdot \mathbf{d}_2 - u_2 \mathbf{d}_1 \cdot \mathbf{d}_2 = u_1 \tag{45}$$

For u_2 and u_3, we similarly obtain $u_2 = -\mathbf{d}_3 \cdot \mathbf{d}_1'$ and $u_3 = -\mathbf{d}_1 \cdot \mathbf{d}_2'$.

The relation between the directors $\mathbf{d}_k$ and the quaternion $\mathbf{q}$ is given in (5). To compute $\mathbf{d}_k'$, we note that $\mathbf{d}_k'$ is a function of $\mathbf{q}$ and $\mathbf{q}$ is a function of the curve parameter σ:

$$\mathbf{d}_k' = \mathbf{d}_k'(\mathbf{q}(\sigma)) = \frac{\partial \mathbf{d}_k(\mathbf{q}(\sigma))}{\partial \sigma} = \frac{\partial \mathbf{d}_k}{\partial \mathbf{q}} \frac{\partial \mathbf{q}}{\partial \sigma} = \mathbf{J}_k \mathbf{q}' \tag{46}$$

where we employed the chain rule of partial differentiation. $\mathbf{J}_k$ is the Jacobi matrix $\mathbf{J}_k = \frac{\partial \mathbf{d}_k}{\partial \mathbf{q}}$ that is obtained by symbolic differentiation. For u_1, we now write

$$u_1 = -\mathbf{d}_2 \cdot \mathbf{J}_3 \mathbf{q}' = -\mathbf{J}_3^\mathsf{T} \mathbf{d}_2 \cdot \mathbf{q}' \tag{47}$$

which results from applying basic linear algebra identities. Similar expressions are obtained for u_2 and u_3. To bring (47) to the desired form (6), we symbolically evaluate the product $\mathbf{J}_3^\mathsf{T} \mathbf{d}_2$ to obtain

$$\mathbf{J}_3^\mathsf{T} \mathbf{d}_2 = \frac{2}{\|\mathbf{q}\|^2} \begin{pmatrix} q_4 & q_3 & -q_2 & -q_1 \end{pmatrix}^\mathsf{T} = \frac{2}{\|\mathbf{q}\|^2} \mathbf{B}_1 \mathbf{q} \tag{48}$$

with the skew-symmetric matrix $\mathbf{B}_1$

$$\mathbf{B}_1 = \begin{pmatrix} 0 & 0 & 0 & 1 \\ 0 & 0 & 1 & 0 \\ 0 & -1 & 0 & 0 \\ -1 & 0 & 0 & 0 \end{pmatrix}$$

The strain rate u_1 can then be obtained by combining (47) and (48). The matrices $\mathbf{B}_2$ and $\mathbf{B}_3$ are obtained in a similar manner as

$$\mathbf{B}_2 = \begin{pmatrix} 0 & 0 & -1 & 0 \\ 0 & 0 & 0 & 1 \\ 1 & 0 & 0 & 0 \\ 0 & -1 & 0 & 0 \end{pmatrix}, \quad \mathbf{B}_3 = \begin{pmatrix} 0 & 1 & 0 & 0 \\ -1 & 0 & 0 & 0 \\ 0 & 0 & 0 & 1 \\ 0 & 0 & -1 & 0 \end{pmatrix}$$

The skew-symmetric matrices $\mathbf{B}_k$ and the resulting vectors $\mathbf{B}_k \mathbf{q}$ have several important properties that are discussed in [Dic94]. A similar analysis [Dic94] can be done to obtain the angular velocities ω_k^0 with respect to the reference frame, resulting in matrices $\mathbf{B}_k^0$:

$$\mathbf{B}_1^0 = \begin{pmatrix} 0 & 0 & 0 & 1 \\ 0 & 0 & -1 & 0 \\ 0 & 1 & 0 & 0 \\ -1 & 0 & 0 & 0 \end{pmatrix}, \quad \mathbf{B}_2^0 = \begin{pmatrix} 0 & 0 & 1 & 0 \\ 0 & 0 & 0 & 1 \\ -1 & 0 & 0 & 0 \\ 0 & -1 & 0 & 0 \end{pmatrix}$$

and

$$\mathbf{B}_3^0 = \begin{pmatrix} 0 & -1 & 0 & 0 \\ 1 & 0 & 0 & 0 \\ 0 & 0 & 0 & 1 \\ 0 & 0 & -1 & 0 \end{pmatrix}$$

Appendix B: Material parameters

	Ropes	Wires	Threads
Length [m]	10	0.1	1
Radius r [m]	0.01	0.001	0.001
Density ρ [kg m^{-3}]	1300	7860	1300
Young modulus E [MPa]	0.5	200	10^{-5}
Shearing modulus G [MPa]	0.5	100	10^{-5}
Stretch modulus E_s [MPa]	20	100	0.02
Spring const. κ [10^3 kg m s^{-2}]	100	300	0.1
γ_t [10^{-6} kg m^3 s^{-1}]	10	0.05	1
γ_r [10^{-6} kg m^3 s^{-1}]	1	0.01	0.1

Table 2: *Material parameters for the objects simulated in the experiments. The parameter values have been determined by visually comparing the behavior of the simulated objects to their real counterparts.*